Journal of Alloys and Compounds 504 (2010) 65–69

Contents lists available at ScienceDirect

Journal of Alloys and Compounds

journal homepage: www.elsevier.com/locate/jallcom

Solid-state phase equilibria in the Co–Pt–Dy ternary system at 1173 K

Gu Zhengfei, Li Ruifeng*, Cheng Gang, Zheng Fuqiang, Wu Yong, Deng Ting

Faculty of Material Science and Engineering, Guilin University of Electronic Technology, Guilin 541004, PR China

ARTICLE INFO

Article history:
Received 28 February 2010
Received in revised form 16 May 2010
Accepted 21 May 2010
Available online 2 June 2010

Keywords:
Transition metal compounds
Rare-earth compounds
Phase diagram
Crystal structure
X-ray diffraction

ABSTRACT

The solid-state phase equilibria in the Co–Pt–Dy ternary system at 1173 K (Dy ≤ 70%) were investigated by X-ray diffraction (XRD), scanning electron microscopy (SEM) and energy dispersion spectroscopy (EDS) techniques. The 1173 K isothermal section consists of 14 single-phase regions, 24 two-phase regions, 10 three-phase regions and 1 four-phase region. At 1173 K, we have observed that the maximum solubility of Dy in α-(Co, Pt) is below 1.5 at.% Dy. The maximum solid solubility of Pt in $Co_{17}Dy_2$ is below 1 at.% Pt, whereas in Co_7Dy_2, Co_3Dy and Co_2Dy is about 1, 1 and 1.5 at.% Pt, respectively. The maximum solid solubility of Co in $DyPt_5$, $DyPt_3$, Dy_3Pt_4, DyPt, Dy_5Pt_4, Dy_5Pt_3, Dy_2Pt and Dy_3Pt is below 1 at.% Co, with uniquely being 19 at.% Co in $DyPt_2$. In this work, one four-phase region including α-(Co, Pt), DyPt, $DyPt_2$, and Dy_3Pt_4 phases was found. Co_5Dy and any new ternary compounds were not observed.

1. Introduction

The Co–Pt, Dy–Pt and Co–Dy binary systems bounding the Co–Pt–Dy ternary system have been widely studied. It has been reported that Co and Pt are mutually soluble with each other in the Co–Pt binary system approximately from 1100 to 1700 K [1]. The phase diagram of Co–Dy binary system was reported by Buschow [2]. At 1173 K, there are four intermetallic compounds, namely $Co_{17}Dy_2$ ($Ni_{17}Th_2$ structure type), Co_7Dy_2 (Co_7Er_2 structure type), Co_3Dy (Be_3Nb structure type) and Co_2Dy (Cu_2Mg structure type). Furthermore, one phase, Co_5Dy ($CaCu_5$ structure type), is unstable according to Ref. [2] and have a tendency to decompose into the two neighboring compounds $Co_{17}Dy_2$ and Co_7Dy_2 below 1403 K. The Dy–Pt binary phase diagram constructed largely on the basis of the presumed similarity with the Er–Pt system was reported in the literature [3], and at 1173 K, it has been confirmed in Ref. [4] that Dy_3Pt (Fe_3C structure type), Dy_2Pt (Co_2Si structure type), Dy_5Pt_3 (Mn_5Si_3 structure type), Dy_5Pt_4 (Ge_4Sm_5 structure type), DyPt (BFe structure type), Dy_3Pt_4 (Pd_4Pu_3 structure type), $DyPt_2$ ($MgCu_2$ structure type), $DyPt_3$ ($AuCu_3$ structure type) and $DyPt_5$ ($SmPt_5$ structure type) were found present in the Fe–Pt–Dy ternary system. Crystallographic data for these binary compounds of the Co–Dy and Dy–Pt systems are collected in Table 1.

However, the study about the Co–Pt–Dy ternary system itself is comparatively scarce up to now. We present here a systematic experimental investigation of the isothermal section of this system at 1173 K so as to reveal the phase equilibria relationship.

2. Experimental

The solid-state phase equilibria in the Co–Pt–Dy system at 1173 K were constructed by using the results of the X-ray phase analysis of 56 samples, as well as those obtained from scanning electron microscopy and energy dispersion spectroscopy on some selected samples. All the samples were prepared by arc-melting of pure metals (the purity of the ingredients is better than 99.9 wt.%) on a water-cooled copper hearth under the protection of pure argon atmosphere. They were remelted at least four times to ensure adequate homogeneity. The mass losses after the melting were less than 0.5 wt.%. After melting, the samples were sealed in vacuum quartz tubes and annealed at 1173 K for 15 days in order to reach good homogeneity, then quenched into ice-water. The brittle samples were ground to powders in a carnelian mortar for X-ray diffraction. A few tough samples were pressed into slices (7 mm × 3mm × 1 mm) and sealed again in vacuum quartz tubes, then annealed at 1173 K for 15 days to ensure homogeneity and eliminate the stress with further being quenched in ice-water for X-ray diffraction. The samples in the Co-rich region were crumbled to particles in a stainless steel mortar, then ground to powders in a carnelian mortar, and finally annealed under the protection of purified argon at 1173 K for 20 h to eliminate the stress and quenched in ice-water for X-ray diffraction. Phase analysis was carried out using X-ray diffraction (Cu Kα radiation), scanning electron microscopy and energy dispersion spectroscopy techniques.

3. Results and discussion

3.1. Phase analysis

3.1.1. Binary Co–Dy system

According to Ref. [2], Co_5Dy was considered as a high temperature phase, it would decompose into $Co_{17}Dy_2$ and Co_7Dy_2 with the eutectoid decomposition temperature of approximately 1403 K. And in Ref. [14], it was reported that the decomposition tempera-

* Corresponding author.
E-mail address: liruifeng8107@163.com (L. Ruifeng).

0925-8388/$ – see front matter © 2010 Elsevier B.V. All rights reserved.
doi:10.1016/j.jallcom.2010.05.109

Table 1
Crystallographic data for the binary compounds of the Co–Dy, Dy–Pt systems.

Compounds	Structure type	Space group	Lattice parameters (nm)			References
			a	*b*	*c*	
$Co_{17}Dy_2$	$Ni_{17}Th_2$	$P6_3/mmc$	0.835	–	0.812	[2,5]
Co_7Dy_2	Co_7Er_2	$R\bar{3}m$	0.4998	–	3.622	[2,6]
Co_3Dy	Be_3Nb	$R\bar{3}m$	0.4999	–	2.436	[2,7]
Co_2Dy	Cu_2Mg	$Fd\bar{3}m$	0.7176	–	–	[2,8]
$DyPt_5$	$SmPt_5$	O^*72	0.5237	0.9098	2.647	[9,10]
$DyPt_3$	$AuCu_3$	$Pm\bar{3}m$	0.407232	–	–	[11]
$DyPt_2$	Cu_2Mg	$Fd\bar{3}m$	0.759667	–	–	[11]
Dy_3Pt_4	Pd_4Pu_3	$R\bar{3}$	1.3107	–	0.5673	[11]
DyPt	FeB	*Pnma*	0.54661	0.445313	0.71189	[11]
DyPt	FeB	*Pnma*	0.6983	0.4478	0.5544	[12]
DyPt	FeB	*oP*8	0.69736	0.44796	0.55391	[13]
Dy_5Pt_4	Ge_4Sm_5	*Pnma*	0.74525	1.45338	0.75265	[11]
Dy_5Pt_4	Ge_4Sm_5	*oP*36	0.7470	1.4560	0.7543	[13]
Dy_5Pt_3	Mn_5Si_3	$P6_3/mcm$	0.83674	–	0.62107	[11]
Dy_5Pt_3	Mn_5Si_3	*hP*16	0.8359	–	0.6233	[13]
Dy_2Pt	Co_2Si	*Pnma*	0.71017	0.47474	0.87318	[11]
Dy_2Pt	Co_2Si	*oP*12	0.70955	0.47392	0.87301	[13]
Dy_3Pt	Fe_3C	*Pnma*	0.70493	0.94855	0.64173	[11]
Dy_3Pt	Fe_3C	*oP*16	0.70421	0.94714	0.64215	[13]

ture of Co_5Dy is near 1173 K. In our work, no diffraction peaks of Co_5Dy were found through careful analysis of the XRD patterns of the Co_5Dy alloy, which proved that Co_5Dy had completely decomposed into $Co_{17}Dy_2$ and Co_7Dy_2 at 1173 K. Moreover, Co_5Dy was not observed in the Co–Pt–Dy ternary system after the introduction of platinum under our experimental condition.

3.1.2. Binary Dy–Pt system

Previous research has found that all the light rare-earth metals (atomic number < 63) form Cu_2Mg-type intermediate phases of RPt_3, but for the heavy rare-earth Tb and Dy, $TbPt_3$ and $DyPt_3$ form $AuCu_3$-type structure [15]. In our work, we have observed that the phase $DyPt_3$ exists with the $AuCu_3$-type structure, which is in good agreement with previous work [15].

For the phase Dy_3Pt_4, it was confirmed that Dy_3Pt_4 compound exists in the Fe–Pt–Dy ternary system at 1173 K [4]. As for the Co–Pt–Dy ternary system, the X-ray diffraction of sample $Co_{45}Pt_{30}Dy_{25}$ in Fig. 1(a) clearly shows the diffraction peaks of Dy_3Pt_4, which implies that the phase Dy_3Pt_4 also exists in the Co–Pt–Dy ternary system. This is different from the phase Pr_3Pt_4 and Nd_3Pt_4 which are unstable and would decompose totally into the two neighboring compounds RPt and RPt_2 (R = Pr, Nd) with the addition of more than 1 at.% Co for the former and 5 at.% Co for the latter [16,17]. The reason for this may be the fact that Dy belongs to heavy rare earth which results in a comparatively smaller atomic radius. It could be tentatively assumed that the R_3Pt_4 (R = Pr, Nd, Dy) phase will be more stable at 1173 K with the decrease of the atomic radius of rare earth.

3.1.3. Ternary Co–Pt–Dy system

In our experiment, it is amazed to see that one four-phase equilibrium region exists in the Co–Pt–Dy system at 1173 K, while no such existence had been observed either in the Co–Pt–R system [16,17] or the Fe–Pt–R system [4,18,19]. Fig. 1(a) and (b) shows, respectively, the X-ray diffraction data and the SEM image of the sample $Co_{45}Pt_{30}Dy_{25}$ which belongs to the four-phase region. The existence of four phases, α-(Co, Pt), $DyPt_2$, Dy_3Pt_4 and DyPt can be clearly observed. To confirm this, the same sample was further put through an annealing process of 1 month at 1173 K. As a result, after re-annealing, the X-ray diffraction data of the sample were almost the same. This indicates that the existence of the four-phase region is stable at 1173 K. However, when the sample $Co_{45}Pt_{30}Dy_{25}$ was annealed at 1273 K for 7 days, it was observed from the X-ray diffraction data (Fig. 2(a)) and the SEM image (Fig. 2(b)) that only three phases α-(Co, Pt), $DyPt_2$, and DyPt are present. This means that the sample in the four-phase region has transformed

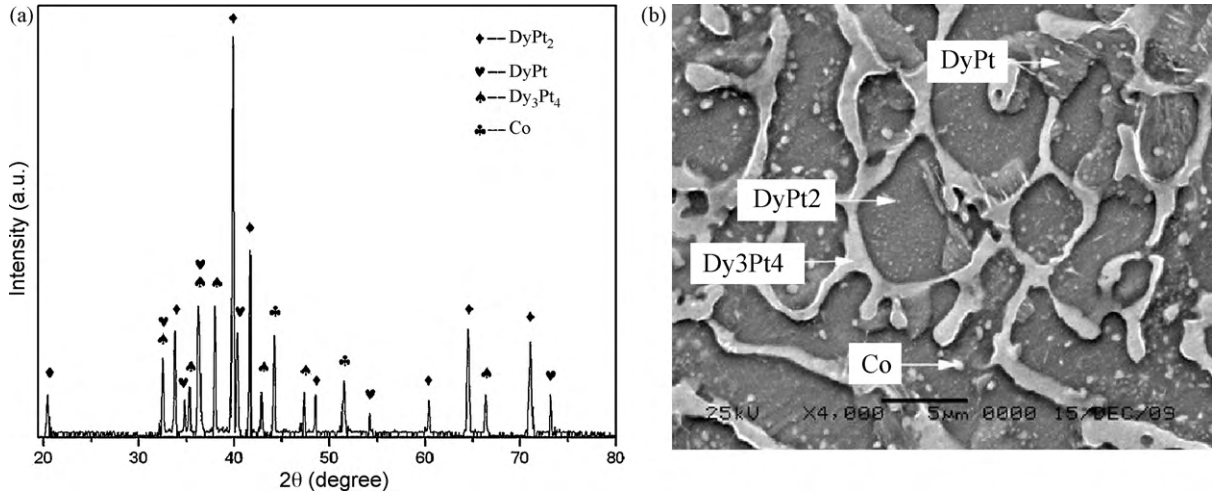

Fig. 1. (a) X-ray pattern and (b) SEM image of $Co_{45}Pt_{30}Dy_{25}$ sample annealed at 1173 K for 15 days.

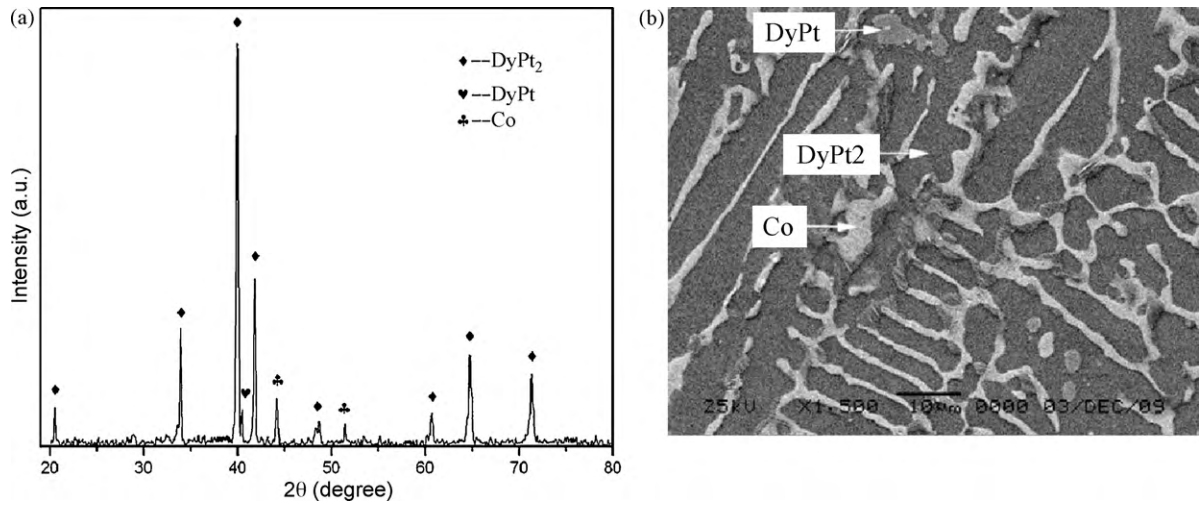

Fig. 2. (a) X-ray pattern and (b) SEM image of $Co_{45}Pt_{30}Dy_{25}$ sample annealed at 1273 K for 7 days.

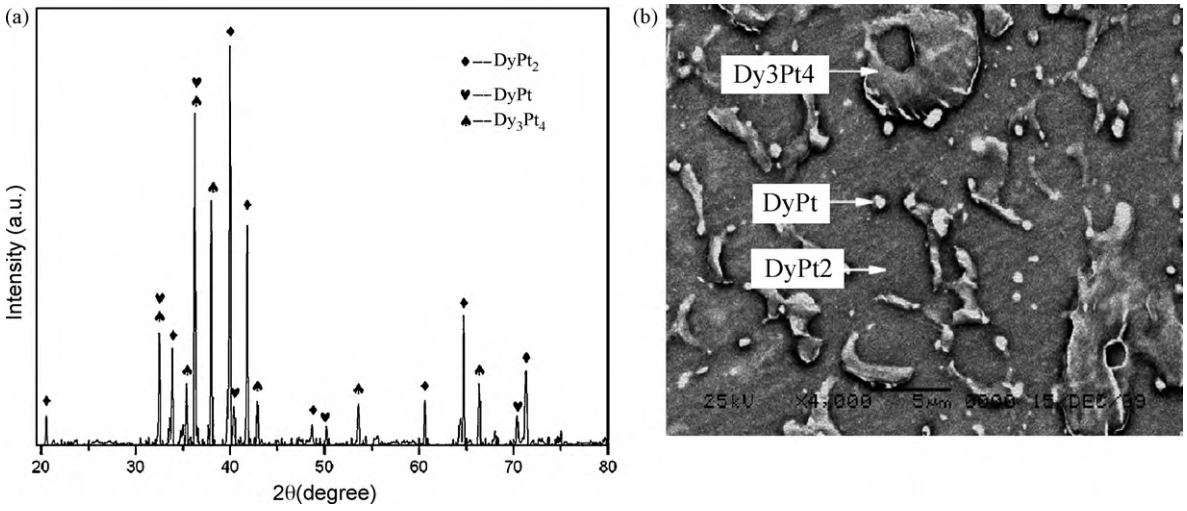

Fig. 3. (a) X-ray pattern and (b) SEM image of $Co_{10}Pt_{50}Dy_{40}$ sample annealed at 1273 K for 7 days.

into one in the three-phase region at 1273 K. However, the sample $Co_{10}Pt_{50}Dy_{40}$ located in the same four-phase region was observed to be converted into one in another three-phase region DyPt, $DyPt_2$ and Dy_3Pt_4 after annealing at 1273 K for 7 days, as shown in Fig. 3(a) and (b). Fig. 4(a) and (b) illustrates the transition of phase region under the annealing temperature of 1173 and 1273 K. From this we could see clearly that the rising of the annealing temperature from 1173 to 1273 K is followed by the formation of two three-phase regions from the original four-phase region, which consists of α-(Co, Pt), DyPt, $DyPt_2$, and DyPt, $DyPt_2$, Dy_3Pt_4, respectively.

3.2. Solid solubility

At 1173 K, by using X-ray diffraction, scanning electron microscopy and energy dispersion spectroscopy techniques, we have observed that the maximum solubility of Dy in α-(Co, Pt) is below 1.5 at.% Dy; the maximum solid solubility of Pt in $Co_{17}Dy_2$ is below 1 at.% Pt, whereas in Co_7Dy_2, Co_3Dy and Co_2Dy is, respectively, about 1, 1 and 1.5 at.% Pt; the maximum solid solubility of Co in $DyPt_5$, $DyPt_3$, Dy_3Pt_4, DyPt, Dy_5Pt_4, Dy_5Pt_3, Dy_2Pt and Dy_3Pt is below 1 at.% Co. But, the maximum linear solid solubility of Co in $DyPt_2$ was determined to be nearly 19 at.% Co under our experimental condition by means of lattice parameter method. Fig. 5(a)–(d) presents the results of the X-ray diffraction data for a series of sam-

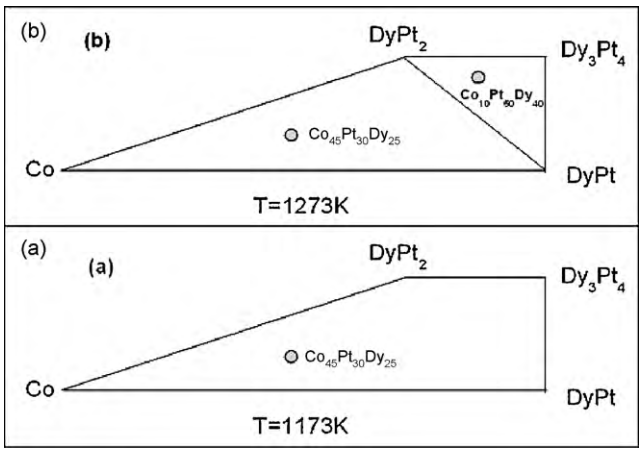

Fig. 4. (a) $Co_{45}Pt_{30}Dy_{25}$ sample in four-phase region (including α-(Co, Pt), $DyPt_2$, DyPt and Dy_3Pt_4) annealed at 1173 K for 15 days; (b) $Co_{45}Pt_{30}Dy_{25}$ in three-phase region (including α-(Co, Pt), $DyPt_2$ and DyPt) and $Co_{10}Pt_{50}Dy_{40}$ in three-phase region (including $DyPt_2$, Dy_3Pt_4 and DyPt) annealed at 1273 K for 7 days.

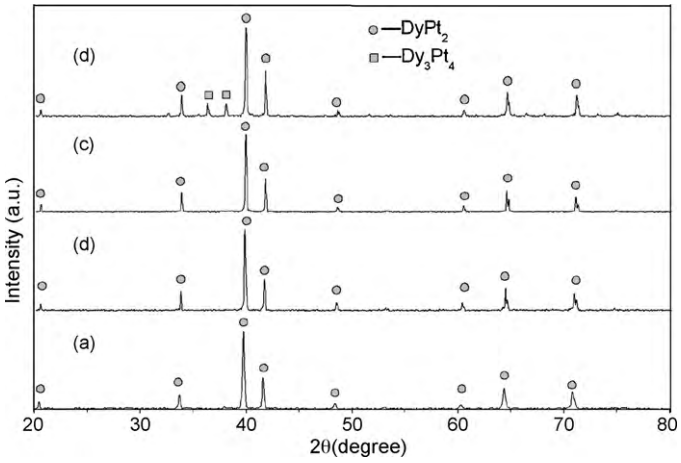

Fig. 5. Observed XRD pattern of the $Co_8Pt_{58.67}Dy_{33.33}$ (a), $Co_{15}Pt_{51.67}Dy_{33.33}$ (b), $Co_{18}Pt_{48.67}Dy_{33.33}$ (c) and $Co_{21}Pt_{45.67}Dy_{33.33}$ (d) compounds annealed at 1173 K for 15 days.

ples $Co_xPt_{66.67-x}Dy_{33.33}$ with $x = 8$, 15, 18 and 21. We can see that with $x = 8$, 15 or 18, the samples are single-phase of $DyPt_2$, but with $x = 21$, addition of Co into the $DyPt_2$ and Dy_3Pt_4 phase can be observed in the $Co_{21}Pt_{45.67}Dy_{33.33}$ sample. According to the data we calculate the lattice parameter of the investigated samples and the results are shown in Fig. 6 as a solid line. It displays that the lattice parameters decreases monotonously with increasing the Co content due to the fact that Co atom has a rather smaller atomic radii than the Pt atom. In addition, a horizontal dash dot line in Fig. 6 presents the lattice parameters of the constituent phase $DyPt_2$ of the samples situated in the $DyPt_2$, DyPt, Dy_3Pt_4 and Co four-phase region, which remains constant. The solubility limit of Co in $DyPt_2$ is the concentration that corresponds to intersection of the solid line and the dash dot line as shown in Fig. 6, which is about 19 at.% Co. The reason for this is quite similar to that of the solubility of Co in $PrPt_5$ and $NdPt_5$ [16,17]. The large solubility limit to which Co dissolves in $DyPt_2$ may be ascribed to several feature of the Co and Pt atoms as follows. Firstly, the Co atom has a rather smaller atomic radii of 0.125 nm than the Pt atom, which is 0.139 nm [20], which brings about a 10% difference. Secondly, Co and Pt (1173 K) have the same face-centered cubic structures. Furthermore, their most common valence is both +2 with a similar electronegativity of 2.2 and 1.8 [20]. Finally, $DyPt_2$ and Co_2Dy share the same Cu_2Mg-type

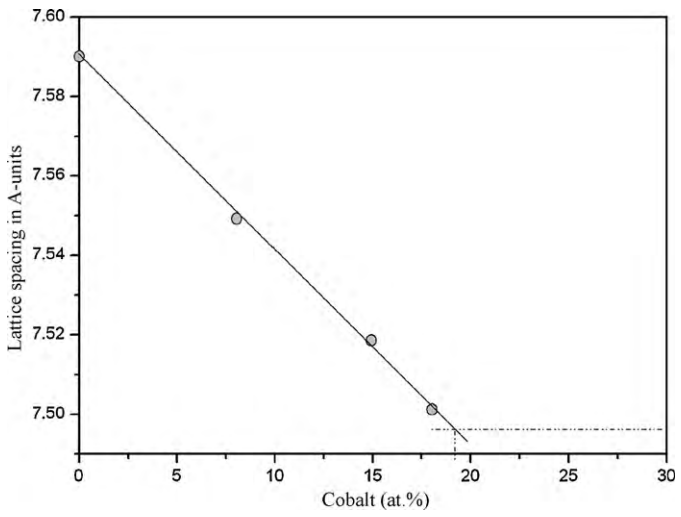

Fig. 6. The variation of the *a*-spacing with at.% Co for some Cu_2Mg-type Co–Pt–Dy alloys.

Table 2
Identification of phase for the ternary alloy.

Samples	Ternary alloys	Phase compositions
1	$Co_{33}Pt_{15}Dy_{52}$	$Dy_3Pt + Dy_2Pt + Co_2Dy$
2	$Co_{42}Pt_{15}Dy_{43}$	$Dy_5Pt_4 + Dy_5Pt_3 + Co_2Dy$
3	$Co_{45}Pt_{15}Dy_{40}$	$Dy_5Pt_4 + DyPt + Co_2Dy$
4	$Co_{57}Pt_{10}Dy_{33}$	$Co_3Dy + Co_2Dy + DyPt$
5	$Co_{67}Pt_{10}Dy_{23}$	$Co_{17}Dy_2 + Co_7Dy_2 + DyPt$
6	$Co_{83}Pt_5Dy_{12}$	α-(Co, Pt) + $Co_{17}Dy_2$ + DyPt
7	$Co_{50}Pt_{30}Dy_{20}$	α-(Co, Pt) + $DyPt_2$
8	$Co_{77}Pt_{20}Dy_3$	α-(Co, Pt) + $DyPt_3$ + $DyPt_2$
9	$Co_{45}Pt_{40}Dy_{15}$	α-(Co, Pt) + $DyPt_3$ + $DyPt_2$
10	$Co_{65}Pt_{30}Dy_5$	α-(Co, Pt) + $DyPt_3$
11	$Co_{48}Pt_{50}Dy_2$	α-(Co, Pt) + $DyPt_3$
12	$Co_{20}Pt_{70}Dy_{10}$	α-(Co, Pt) + $DyPt_3$
13	$Co_{28}Pt_{69}Dy_3$	α-(Co, Pt) + $DyPt_5$ + $DyPt_3$
14	$Co_{15}Pt_{75}Dy_{10}$	α-(Co, Pt) + $DyPt_5$ + $DyPt_3$
15	$Co_{17}Pt_{81}Dy_2$	α-(Co, Pt) + $DyPt_5$
16	$Co_{15}Pt_{51.67}Dy_{33.3}$	$DyPt_2$
17	$Co_{18}Pt_{48.67}Dy_{33.3}$	$DyPt_2$
18	$Co_{21}Pt_{45.67}Dy_{33.3}$	α-(Co, Pt) + $DyPt_2$ + Dy_3Pt_4 + DyPt
19	$Co_{15}Pt_{50}Dy_{35}$	$DyPt_2$ + Dy_3Pt_4
20	$Co_{10}Pt_{50}Dy_{40}$	α-(Co, Pt) + $DyPt_2$ + Dy_3Pt_4 + DyPt
21	$Co_{15}Pt_{45}Dy_{40}$	α-(Co, Pt) + $DyPt_2$ + Dy_3Pt_4 + DyPt
22	$Co_{30}Pt_{40}Dy_{30}$	α-(Co, Pt) + $DyPt_2$ + Dy_3Pt_4 + DyPt
23	$Co_{45}Pt_{30}Dy_{25}$	α-(Co, Pt) + $DyPt_2$ + Dy_3Pt_4 + DyPt
24	$Co_8Pt_{58.67}Dy_{33.3}$	$DyPt_2$

structure. Interestingly, the solid solubility of Pt in Co_2Dy is quite different from Co in $DyPt_2$. The most possible reason for this is that Co has smaller atomic radii than Pt and smaller atomic radii makes the formation of solid solution easier.

In Refs. [16,17], it has been reported that the maximum linear solid solubility of Co in $PrPt_5$ and $NdPt_5$ are 15 at.%. However, in our experiment, we have found that there is nearly no solid solubility for $DyPt_5$ upon the addition of Co. The reason for this is very likely due to the fact that the phase Co_5Dy is not present at 1173 K, furthermore, both Co_5Dy ($CaCu_5$ structure type) and $DyPt_5$ ($SmPt_5$ structure type) have totally different structure type. Thus, formation of Dy(Pt, Co)$_5$ can hardly be observed.

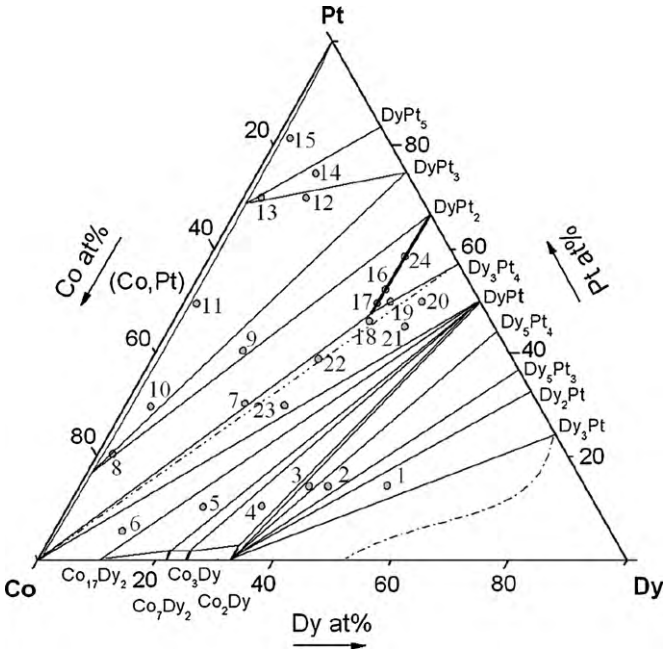

Fig. 7. Isothermal section of the Co–Pt–Dy system at 1173 K.

3.3. Isothermal section at 1173 K

In this work, by comparing and analyzing the X-ray diffraction patterns of 56 samples, together with scanning electron microscopy and energy dispersion spectroscopy on some of the selected samples, we have identified the phase components and phase relations of each sample (in Table 2). According to these results, the solid-state phase equilibria of Co–Pt–Dy system at 1173 K ($Dy \leq 70\%$) were determined. The 1173 K isothermal section shown in Fig. 7 consists of 14 single-phase regions α(α-(Co, Pt)), β($Co_{17}Dy_2$), γ(Co_7Dy_2), δ(Co_3Dy), ε(Co_2Dy), ζ(Dy_3Pt), η(Dy_2Pt), θ(Dy_5Pt_3), ι(Dy_5Pt_4), κ(DyPt), λ(Dy_3Pt_4), μ($DyPt_2$), ν($DyPt_3$), ξ($DyPt_5$), 24 two-phase regions (α + ξ, α + ν, α + μ, μ + λ, α + β, β + γ, γ + δ, δ + ε, ζ + η, η + θ, θ + ι, ι + κ, κ + λ, μ + ν, ν + ξ, α + κ, β + κ, γ + κ, δ + κ, ε + κ, ε + ι, ε + θ, ε + η, ε + ζ), 10 three-phase regions (α + ν + ξ, α + μ + ν, α + κ + β, κ + γ + β, κ + δ + γ, ε + ζ + η, ε + η + θ, ε + θ + ι, ε + ι + κ, κ + ε + δ) and one four-phase region (α + μ + κ + λ).

4. Conclusion

(1) At 1173 K, the Co_5Dy phase was not found in the Co–Pt–Dy ternary system; the $DyPt_3$ phase with the $AuCu_3$-type structure exists in the Dy–Pt binary system; the Dy_3Pt_4 phase remains stable with the addition of the Co element.
(2) One four-phase equilibrium region including α-(Co, Pt), $DyPt_2$, Dy_3Pt_4 and DyPt exists in the Co–Pt–Dy system at 1173 K.
(3) The maximum solubility of Dy in α-(Co, Pt) is below 1.5 at.% Dy, the maximum solid solubility of Pt in $Co_{17}Dy_2$ is below 1 at.% Pt, and in Co_7Dy_2, Co_3Dy and Co_2Dy is about 1, 1 and 1.5 at.% Pt, respectively; the maximum solid solubility of Co in $DyPt_5$, $DyPt_3$, Dy_3Pt_4, DyPt, Dy_5Pt_4, Dy_5Pt_3, Dy_2Pt and Dy_3Pt is below 1 at.% Co and that of Co in $DyPt_2$ is 19 at.% Co.
(4) The 1173 K isothermal section of the phase diagram of the Co–Pt–Dy ternary system consists of 14 single-phase regions, 24 two-phase regions, 10 three-phase regions and 1 four-phase region. No new ternary compounds were observed.

Acknowledgement

This work was supported by the National Natural Science Foundation of China (authorized numbers: 50261002 and 50661002).

References

[1] T. Massalsky (Ed.), Binary Alloy Phase Diagrams, 2nd ed., ASM International, Materials Park, OH, 1996.
[2] K.H.J. Buschow, Philips Res. Rep. 26 (1971) 49.
[3] T.B. Massalski (Ed.), Binary Alloy Phase Diagrams, 2nd ed., ASM International, Materials Park, OH, 1990.
[4] L. Ma, Z.F. Gu, X.P. Zhong, G. Cheng, B. Zhou, C.F. Xu, J. Alloys Compd. 427 (2007) 130–133.
[5] R.J. Radwanski, H. Figiel, K. Krop, S. Warchol, Solid State Commun. 41 (12) (1982) 921–923.
[6] C.H. Wu, L.G. Yao, Y.C. Chuang, Zeitschrift Fuer Metallkd. 85 (1994) 104–108.
[7] W. Stertag, Trans. Metall. Soc. Aime 239 (1967) 690–694.
[8] M.I. Slanicka, K.N.R. Taylor, G.J. Primavesi, J. Phys. F: Metal Phys. 1 (1971) 679–685.
[9] B. Erdmann, C. Keller, J. Solid State Chem. 7 (1973) 40–48.
[10] W. Bronger, J. Less-Common Met. 12 (1) (1967) 63–68.
[11] P. Villars, L.D. Calvert, Pearson's Handbook of Crystallographic Data for Intermetallic Phases, ASM International, Materials Park, OH, 1991.
[12] Powder Diffraction File, International Center for Diffraction Data [M], Pennsylvania, 1993.
[13] D. Maccio, F. Rosalbino, A. Saccone, S. Delfino, J. Alloys Compd. 391 (2005) 60–66.
[14] ZHU Qiming, ZHUANG Yinghong, LIANG Jianlie, J. Rare Earths 27 (2009) 100–103.
[15] L.R. Harris, J. Less-Common Met. 14 (1968) 462.
[16] H. Zhifeng, G. Zhengfei, C. Gang, H. Qingyan, Z. Fuqiang, L. Ruifeng, J. Alloys Compd. 481 (2009) 301–304.
[17] H. Qingyan, G. Zhengfei, C. Gang, H. Zhifeng, J. Alloys Compd. 485 (2009) 497–500.
[18] C.F. Xu, Z.F. Gu, G. Cheng, L. Ma, B. Zhou, J. Alloys Compd. 424 (2006) 128–130.
[19] R. Jing, G. Zhengfei, C. Gang, Z. Huaiying, J. Alloys Compd. 394 (2005) 211–214.
[20] W.D. Callister Jr., Fundamentals of Materials Science and Engineering, 5th ed., Chemical Industry Press (China), Salt Lake City, UT, 2000.